Development of a Piezoelectric based Energy Harvesting System for Autonomous Wireless Sensor Nodes

Andrés Felipe Gomes-Casseres Espinosa, Andrea Sanchez Ramirez, Luis Francisco Combita Alfonso, Richard Loendersloot, Arthur Berkhoff

7th European Workshop on Structural Health Monitoring
July 8-11, 2014. La Cité, Nantes, France

DEVELOPMENT OF A PIEZOELECTRIC BASED ENERGY HARVESTING SYSTEM FOR AUTONOMOUS WIRELESS SENSOR NODES

Andrés Felipe Gomez-Casseres Espinosa[1], Andrea Sanchez Ramirez[2], Luis Francisco Cómbita Alfonso[1], Richard Loendersloot[2], Arthur Berkhoff[2]

[1] *Facultad de Ingeniería, Universidad Distrital Francisco Jose de Caldas. Bogotá, Colombia.*
[2] *Chair of Dynamics Based Maintenance, University of Twente, The Netherlands.*

afgomezc@correo.udistrital.edu.co

ABSTRACT

This paper describes the selection and operation of a *Boost Integrated with Flyback Rectifier/Energy storage/DC-DC* converter (BIFRED) for piezoelectric energy harvesting purposes. This topology presents features like low-harmonic rectification, energy storage and wide-bandwith voltage control in an integrated single converter, leading to fewer components, weight and miniaturization of the entire system. This miniaturization makes the integrated topologies a suitable option for further developments in Wireless Sensor Network based Structural Health and Condition Monitoring applications. The operation of the BIFRED circuit in *Discontinuous Conduction Mode* (DCM) mode is described. A nonlinear model is derived and used to predict the DC gains between the input, storage and output voltages of the circuit. A simulation-based verification is carried out using *MATLAB Simulink*, the operation of the circuit is corroborated and the power factor is computed. Finally, the results of a piezoelectric implementation using the BIFRED circuit are presented.

KEYWORDS : *Piezoelectric sensors, Energy harvesting, autonomous systems, Structural Health Monitoring.*

INTRODUCTION

The development of Smart Wireless Sensors promises significant contributions to the performance monitoring of complex mechanical systems, being these main objectives for Condition Monitoring and Structural Health Systems. The autonomy and embeddedness characteristics of the sensors nodes support their positioning in locations traditionally forbidden for wired sensors, such as rotating blades [1]. However, the main limitations for the development of autonomous wireless sensors lie on the little energy availability at the node surroundings for the functioning of the node in relation to sensing, processing and communication.

The research on this paper is framed in the development of on-blade autonomous sensors for helicopter rotor blade monitoring. The rotating blade environment poses significant challenges, both at the mechanical and the electronics domains. The mechanical restrictions refer to the integration to the host structure with a minimal disruption in terms of weight, size, connectivity, etc. The electronic perspective relates to the low power and therefore the high efficiency for transforming the energy to the requirements of the node. The two sets of constraints are addressed by using energy harvesting system consisting of piezoelectric diaphragms and by a specialized circuit for energy processing. The work presented focuses on the design of an efficient electronics circuit for extraction, processing, storage and delivery of the power generated by a piezoelectric element attached to a vibrating structure to the wireless node.

The piezoelectric element interacts with the strain field of the mechanical structure. The uniformity of such field ensures the actual charge generation by the piezoelectric material. As a circuit element, the piezoelectric behaves as a power source that provides the energy to the circuit, with an intrinsic

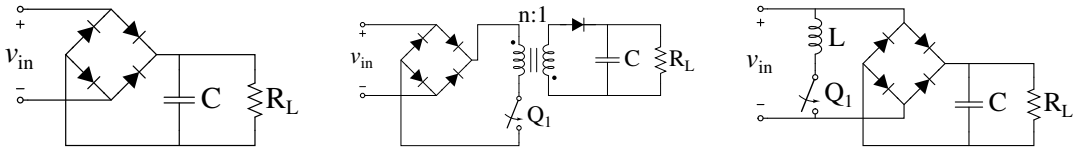

(a) DCIM circuit schematic (b) SECE circuit schematic (c) SSHI circuit schematic

Figure 1 : Previous circuits

capacitance and resistance due to material characteristics [2–4]. The circuit desired must extract efficiently the charge from the piezoelectric material and transform it into an useful form to te load. Power processing is another feature required from the circuit design, since the power generated at the transducer cannot be used directly by node. The circuit needs to display low power losses due to its own operation and meet the requirements imposed by the load. These attributes are summarized as: high Power Factor, high circuit efficiency and possibility for adjusting to the required load.

1. PREVIOUS CIRCUITS

Different circuits have been explored [2] to extract energy from a piezoelectric material. Some of these are the *Direct Current Impedance Matching* (DCIM), the *Synchronous Electric Charge Extraction* (SECE) and the *Synchronized Switch Harvesting on Inductor* (SSHI), which are presented in the figure 1.

In order to select the most suitable circuit to function on an autonomous wireless system a comparison is made between the circuits mentioned above. The evaluation of circuit performance is based on the power factor (PF), need of control and possibility for regulation as seen on Table 1. These parameters are explained below:

- **Power Factor:** The power factor of a power circuit is the ratio between the input average power and the apparent power. This parameter is a measurement of how effectively energy is transmitted between a source and a load network [5].
- **Need of control:** Some power systems require the use of separated control circuitry in order to function properly. This additional system increases the number of components of the overall system.
- **Regulation:** The voltage presented by the power processing circuit to an electrical load must meet certain requirements in order to ensure the well functioning of the load. This requirements should be independent from disturbances inside the circuit. The regulation, supported by a control system, prevents that the disturbance presented in the system impact the behavior of the load.

Table 1 : Qualitative comparison between Energy Harvesting Circuits.

Circuit	PF	Need of control	Regulation
DCIM	Low	No	No
SSHI	High	Yes	No
SECE	High (without regulation)	Yes	Yes (without high PF)

As shown by the Table 1, The SSHI circuit does not allow the regulation of the load voltage. This entails that the output voltage will only depend on the input voltage and prevents to meet load requirements. The DCIM circuit does not need an additional control system (reducing the components of the overall system) but presents a poor PF and a regulation feature is not available, as in the SSHI circuit.

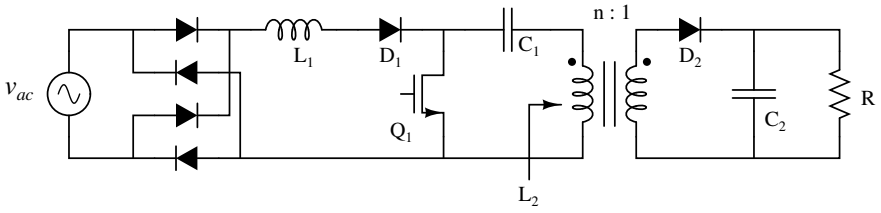

Figure 2 : BIFRED circuit schematic

The low PF implies that most of the energy provided by the source will not reach the load, increasing the power losses within the circuit. The SECE circuit is capable to provide each feature separately.

2. THE BIFRED CIRCUIT

The schematic of a *Boost Integrated with Flyback Rectifier/Energy storage/DC-DC* (BIFRED) converter is shown in the figure 2. A model of the dynamic behavior of the circuit will be derived and the DC voltage gains will be calculated. In order to focus on the BIFRED circuit, a sinusoidal voltage source will represent the voltage generated by the piezoelectric material.
The reason to choose the BIFRED circuit is that it provides all the advantages presented by the previous circuits in a single topology, such as, high power factor and wide-bandwidth regulation. This implies that the BIFRED circuit does not need additional power circuitry to perform tasks needed by the wireless node.

2.1 Operation

A BIFRED circuit operating in *Continuous Conduction Mode* (CCM) presents high capacitor voltages due to the difference between the output and input powers [6, 7]. Therefore a DCM operation mode is selected. To guarantee a high power factor, the current flowing through L_1 must reach zero before the current in L_2 does [6]. This DCM characteristic leads to a four equivalent circuits which are shown in figure 3. It should be noted that each equivalent circuit is the result of replacing the switching components by their equivalent on/off state.

2.2 Analysis

The aim of the following analysis is to obtain a mathematical model that reproduces the dynamic response of the BIFRED circuit in DCM. From this model DC gains between the input, storage and

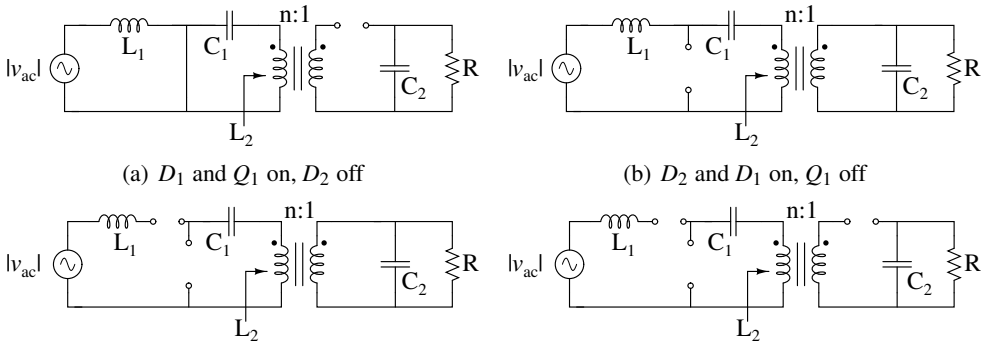

(a) D_1 and Q_1 on, D_2 off

(b) D_2 and D_1 on, Q_1 off

(c) D_2 on, D_1 and Q_1 off

(d) D_1, Q_1 and D_2 off

Figure 3 : Equivalent circuits of the BIFRED converter in DCM

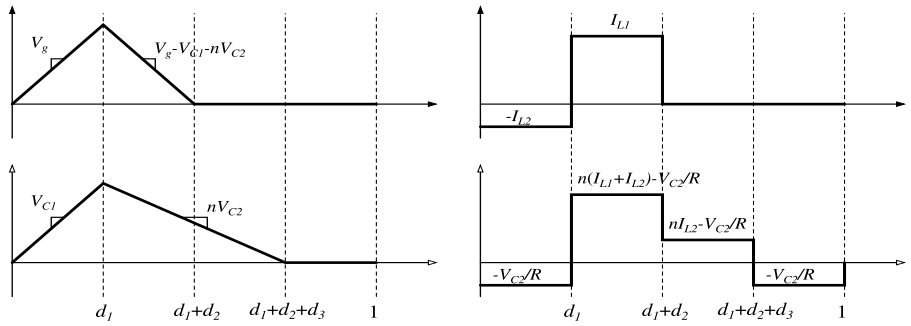

Figure 4 : BIFRED waveforms (the x-axis is t/T_s)

output voltages will be obtained. The analysis is based on the average circuit modeling technique [5] which allows to build a model valid for frequencies much lower than the switching frequency T_s.// Firstly, it is necessary to extract the model directly from the equivalent circuits derived from the BIFRED schematic using the mentioned technique. Secondly, a nonlinear analysis based on [8] will be carried out with the aim of obtaining the static response of the circuit.

2.2.1 Average modeling

In order to obtain an average model from the BIFRED circuit is necessary to extract the waveforms of the voltages on the inductors and the currents through the capacitors within the circuit. This is accomplished using the equivalent circuits shown in the figure 3. The first interval ($0 < t < d_1 T_s$) of the switching period is analyzed. In this interval the MOSFET Q_1 and the diode D_1 are conducting and the diode D_2 is open, obtaining the circuit shown in the figure 3(a). From this circuit and using the Kirchhoff current and voltage law, the coil voltages and capacitor currents in the circuit are shown in the equation (1). Following the same approach, the values for the voltages on the inductors and the currents through the capacitors for the remaining intervals are found and shown in the figure 4.

$$\begin{aligned} v_{L1} &= v_g \\ v_{L2} &= v_{C1} \\ i_{C1} &= -i_{L2} \\ i_{C2} &= -\frac{v_{C2}}{R} \end{aligned} \tag{1}$$

Now that the waveforms of the inductor voltages and the capacitor currents were obtained, it is necessary to obtain their average values over the switching period. Considering that the input voltage and the voltage on the capacitors do not change considerably over T_s; the voltage average over one switching period of the coil voltages is shown in the equations (2). Notice that the average is represented by the triangular brackets and the averaging period is explicitly shown with the T_s subscript.

$$\begin{aligned} \langle v_{L1} \rangle_{T_s} &= d_1 \langle v_g \rangle_{T_s} + d_2 \left(\langle v_g \rangle_{T_s} - \langle v_1 \rangle_{T_s} - n \langle v_2 \rangle_{T_s} \right) + d_6 (0) \\ \langle v_{L2} \rangle_{T_s} &= d_1 \langle v_1 \rangle_{T_s} - d_5 \left(n \langle v_2 \rangle_{T_s} \right) + d_4 (0) \end{aligned} \tag{2}$$

Where $d_4 = 1 - d_3 - d_2 - d_1$, $d_5 = d_2 + d_3$ and $d_6 = d_3 + d_4$ are used to simplify the notation. The approximation made related to the capacitor voltages cannot be applied to the coil currents since, their discontinuous nature avoids the consideration of signals unchangeable in one switching period. To calculate the average value for the currents through the inductors, is necessary to use the general

equation to obtain the DC value of a signal and, noticing that the integral can be calculated applying the formula for the area of a triangle, the equations (3) are obtained.

$$\begin{aligned}\langle i_{C1}\rangle_{T_s} &= \frac{1}{T_s}\left(-\frac{d_1 T_s}{2} i_{2,pk} + \frac{d_2 T_s}{2} i_{1,pk}\right) \\ \langle i_{C2}\rangle_{T_s} &= \frac{1}{T_s}\left(-\frac{v_2}{R} T_s + n\frac{d_2 T_s}{2} i_{1,pk} + n\frac{d_5 T_s}{2} i_{2,pk}\right)\end{aligned} \tag{3}$$

The peak values of the coil currents can be found using the coil voltage, which is proportional to the slope in each interval, multiplied by the interval length, this results in $i_{1,pk} = \frac{d_1 T_s}{L_1}\langle v_g\rangle_{T_s}$ and $i_{2,pk} = \frac{d_1 T_s}{L_2}\langle v_1\rangle_{T_s}$. Substitution of these values into the equations (3) results in the equations (4).

$$\begin{aligned}\langle i_{C1}\rangle_{T_s} &= \frac{d_1 d_2}{2L_1}\langle v_g\rangle_{T_s} - \frac{d_1^2 T_s}{2L_2}\langle v_1\rangle_{T_s} \\ \langle i_{C2}\rangle_{T_s} &= -\frac{1}{R}\langle v_2\rangle_{T_s} + n\frac{d_1 d_2 T_s}{2L_1}\langle v_g\rangle_{T_s} + n\frac{d_1 d_5 T_s}{2L_2}\langle v_1\rangle_{T_s}\end{aligned} \tag{4}$$

The unknown quantities in the equations (4) are d_2 and d_5. These quantities can be found obtaining the average value of the inductor currents [9]. After computation of the average value of the inductor currents and performing some algebraic manipulation, the quantities d_2 and d_5 are obtained and presented in the equations (5).

$$\begin{aligned}d_2 &= \left(\frac{2L_1}{d_1^2 T_s}\frac{\langle i_1\rangle_{T_s}}{\langle v_g\rangle_{T_s}} - 1\right) d_1 \\ d_5 &= \left(\frac{2L_2}{d_1^2 T_s}\frac{\langle i_2\rangle_{T_s}}{\langle v_1\rangle_{T_s}} - 1\right) d_1\end{aligned} \tag{5}$$

With the aim of defining a state space model, it is necessary to define the relations between the derivatives of the state variables. This is presented in the equations (6). The derivation of such model can be found in [5] and is based on the average current-voltage relation of each component.

$$\begin{aligned}L_k\frac{d\langle i_k\rangle_{T_s}}{dt} &= \langle v_{Lk}\rangle_{T_s} \\ C_k\frac{d\langle v_k\rangle_{T_s}}{dt} &= \langle i_{Ck}\rangle_{T_s}\end{aligned} \tag{6}$$

Where $k = \{1,2\}$. Substituting equations (4), (2) and (5) into equations (6), the state space model of the BIFRED converter is obtained and shown in the equations (7).

$$L_1\frac{d\langle i_1\rangle}{dt} = d_1\langle v_g\rangle + \left(\frac{R_{e1}\langle i_1\rangle}{\langle v_g\rangle} - 1\right)(\langle v_g\rangle - \langle v_1\rangle - n\langle v_2\rangle)\, d_1 \tag{7a}$$

$$L_2\frac{d\langle i_2\rangle}{dt} = d_1\langle v_1\rangle - \left(\frac{R_{e2}\langle i_2\rangle}{\langle v_1\rangle} - 1\right) d_1\, n\langle v_2\rangle \tag{7b}$$

$$C_1\frac{d\langle v_1\rangle}{dt} = \langle i_1\rangle - \frac{\langle v_g\rangle}{R_{e1}} - \frac{\langle v_1\rangle}{R_{e2}} \tag{7c}$$

$$C_2\frac{d\langle v_2\rangle}{dt} = n\left(\langle i_1\rangle + \langle i_2\rangle - \frac{\langle v_g\rangle}{R_{e1}} - \frac{\langle v_1\rangle}{R_{e2}}\right) - \frac{\langle v_2\rangle}{R} \tag{7d}$$

Comparing de equations (7) and (5), it can be seem that the factors R_{e1} and R_{e2} are equal to $\frac{2L_1}{d_1^2 T_s}$ and $\frac{2L_2}{d_1^2 T_s}$ respectively. It is important to point out that the subscript T_s is not shown for easier readability of the equations.

2.2.2 DC analysis

The system modeled by the equations (7) is not linear due to the multiplication of the state variables by d_1 and between themselves. The response of such system depends not only on the value of the inputs but on the initial value of the state variables as well. To analyze this type of system is necessary to find the points where the response of the system reaches the steady state or equilibrium points. These points, in the perspective of power circuits, are the DC response of the system. To find the equilibrium points of the model presented in the equations (7) is necessary to set the derivatives to zero. This is shown in the equations (8). Notice that the notation has change in order to emphasize that variables are DC values.

$$0 = D_1 V_g + \left(\frac{R_{e1} I_1}{V_g} - 1\right)(V_g - V_1 - nV_2) D_1 \tag{8a}$$

$$0 = D_1 V_1 - \left(\frac{R_{e2} I_2}{V_1} - 1\right) D_1 nV_2 \tag{8b}$$

$$0 = I_1 - \frac{V_g}{R_{e1}} - \frac{V_1}{R_{e2}} \tag{8c}$$

$$0 = n\left(I_1 + I_2 - \frac{V_g}{R_{e1}} - \frac{V_1}{R_{e2}}\right) - \frac{V_2}{R} \tag{8d}$$

Replacing the DC values of the currents I_1 and I_2 obtained from equations (8c) and (8d) into the equations (8a) and (8b) allow us to find an expression that relates only the voltages V_1 and V_2. The expression is shown in the equation (9).

$$\frac{d_1 R_{e2}}{R}\left(\frac{V_2}{V_1}\right)^2 = d_1 + d_1 n \frac{V_2}{V_1} \tag{9}$$

Performing the substitutions $R_{e2} = \frac{2L_2}{d_1^2 T_s}$, $M_2 = \frac{V_2}{V_1}$ and $K_f = \frac{2L_2}{RT_s}$ on the equation (9), an expression to find the gain or ratio between the dc values V_2 and V_1 is found and shown in the equation (10).

$$M_2^2 - \frac{n d_1^2}{K_f} M_2 - \frac{d_1^2}{K_f} = 0 \tag{10}$$

Following the same methodology, defining $M_1 = \frac{V_1}{V_g}$ and noticing that $\frac{V_1 V_2}{V_g^2} = M_1^2 M_2$ the equation (11) is obtained. This equation models the relation between the DC values V_1 and V_g of the BIFRED circuit.

$$(1 + nM_2) M_1^2 - M_1 - \frac{L_2}{L_1} = 0 \tag{11}$$

3. SIMULATION RESULTS

A DCM BIFRED circuit was designed using the method proposed by [6]. An input low-pass filter with $L_f = 633\,\mu$H and $C_f = 10\,\mu$F was added to improve the power factor of the circuit. The components obtained after the design process are $L_1 = 19.401\,\mu$H, $L_2 = 271.819\,\mu$H, $C_1 = 6.6\,$mF, $C_2 = 3.3\,$mF, $n = 5$ and $R = 500\,\Omega$. Using a duty cycle D of 0.2, the calculated DC gains are $M_1 = 0.8548$ and $M_2 = 3.8691$.

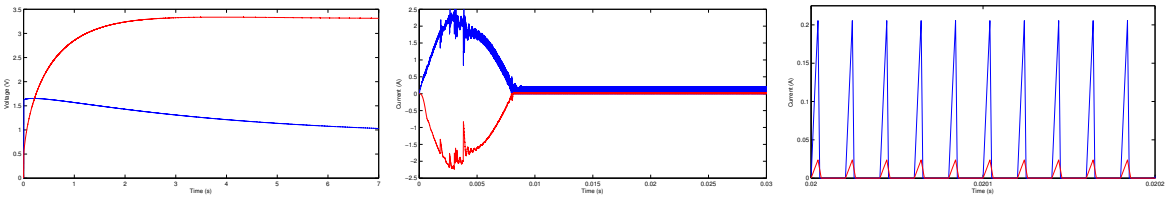

(a) Voltages v_1 (blue) and v_2 (red)

(b) Currents i_1 (blue) and i_2 (red)

(c) Currents i_1 (blue) and i_2 (red) over three switching periods

Figure 5 : Waveforms resulted from the simulation of the BIFRED converter in DCM

The simulation was performed using a DC input voltage value of 1 V. The simulated waveforms of the voltages on C_1 and C_2 and the currents trough L_1 and L_2 are shown un the figures 5. Some parameters were calculated from the simulated waveforms, the values obtained were $PF = 0.99518$, input power $P_i = 26.123\,\text{mW}$, output power $P_o = 21.937\,\text{mW}$, $M_1 = 1.0287$ and $M_2 = 3.2195$. Observe that the operation described previously is verified by the current waveforms shown in figure 5(c).

4. MECHANICAL TEST

Whit the purpose of estimating the output power of a piezoelectric material attached to a vibrating structure, a mechanic setup was built using the M8528P2 from smart-materials. This setup is shown in the figure 6(c). The piezoelectric element is connected to a resistive load of $52\,\text{K}\Omega$ obtained from the maximum power transfer theorem. The voltage on the load and the generated current are shown in the figures 6(a) and 6(b) respectively. The power generated by the piezoelectric element is $113.91\,\mu\text{W}$. The mechanic setup was built using a mechanical shaker, a power amplifier and a glass fiber cantilever with the M8528P2 attached to it. A Polytec OFV303 laser-vibrometer and a Dantec XY motion table were used to measure the displacement developed at different grid points along the cantilever. A NI PXI4472 was used to acquire and store the signals measured from the setup and a NI PXI5412 was used to generate the signal for the shaker.
A second setup was used to observe the response of the BIFRED circuit using a piezoelectric device as a power source. This setup used the same piezoelectric device without a load resistance; the results are shown in the figures 7. The voltage developed by the piezoelectric material is presented in the figure 7(a) and the current flowing through L_1 is presented in the figures 7(b), 7(c) and 7(d).

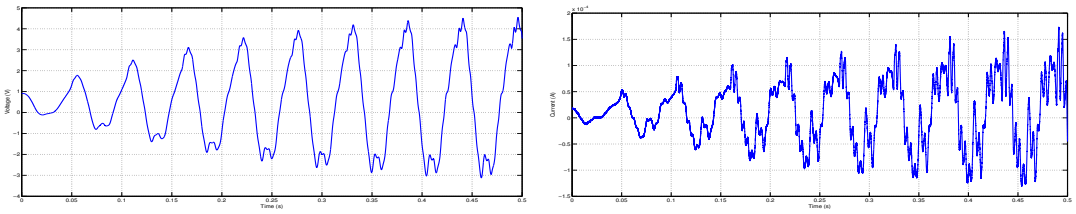

(a) Measured piezoelectric voltage

(b) Piezoelectric current

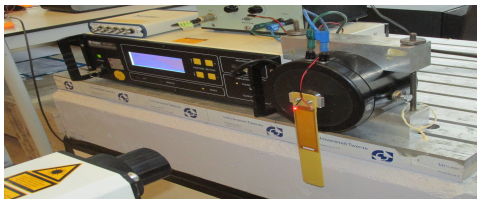

(c) Piezoelectric setup

Figure 6 : Setup and results from the piezoelectric test

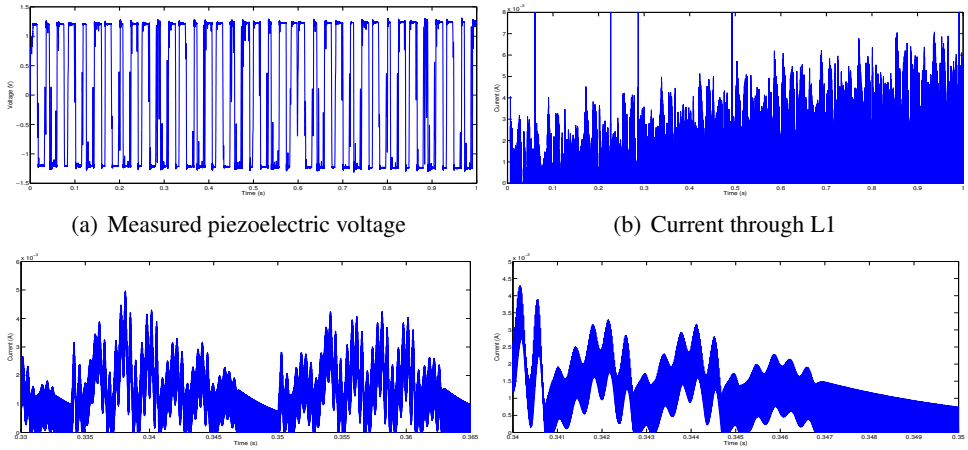

(a) Measured piezoelectric voltage

(b) Current through L1

(c) Current through L1

(d) Current through L1

Figure 7 : Results from the piezoelectric test using the BIFRED circuit

5. CONCLUSION

A qualitative comparison between the circuits used by [2] was performed using three requirements imposed by a wireless node implementation,
A verification of the DCM BIFRED circuit using a DC supply and a piezoelectric element as a power source was performed. As shown in figure 7(d), the current through L_1 is conformed by the expected current peaks on top of undesirable low frequencies sinusoids. These low frequency sinusoids are generated by the piezoelectric material and change the operation mode of the circuit. More studies about the impact on the performance should be carried.
A nonlinear model for the BIFRED circuit is presented and used to predict the DC gains between the input, storage and output voltages. It has been found that the value of the DC gains only depend on the operation mode of the circuit (DCM or CCM), which is established only by the values selected for the inductors of the circuit.
The operation in DCM mode of the BIFRED was verified. The power factor was calculated from the simulated waveforms, showing values near to 1. Further implementation is required to verify the efficiency of the circuit.

REFERENCES

[1] Andrea Sanchez Ramirez, Kallol Das, Richard Loendersloot, Tiedo Tinga, and Paul Havinga. Wireless Sensor Network for Helicopter Rotor Blade Vibration Monitoring: Requirements Definition and Technological Aspects.

[2] Pieter de Jong. *Power Harvesting Using Piezoelectric Materials*. PhD thesis, University of Twente, 2013.

[3] A. H. Meitzler, D. Berlincourt, F. S. Welsh, H. F. Tiersten, G. A. Coquin, and A. G. Warner. IEEE Standard on Piezoelectricity. Technical report, IEEE, 1987.

[4] Ramon Pallàs-Areny and J. G. Webster. *Sensors and signal conditioning*. 2001.

[5] Robert W. Erickson and Dragan Maksimović. *Fundamentals of Power Electronics*.

[6] Michael J. Willers, Michael G. Egan, Seamus Daly, and John M. D. Murphy. Analysis and Design of a Practical Discontinuous-Conduction-Mode BIFRED Converter.

[7] M. J. Willers, M. G. Egan, J. M. D. Murphy, and S. Daly. A BIFRED converter with a wide load range.

[8] S Strogatz. *Nonlinear Dynamics and Chaos: With Applications to Physics, Biology, Chemistry and Engineering*. Addison-Wesley, 1994.

[9] Jian Sun, Daniel M. Mitchell, Matthew F. Greuel, Philip T. Krein, and Richard M. Bass. Averaged Modeling of PWM Converters Operating in Discontinuous Conduction Mode.